Current Biology, Volume *32*

Supplemental Information

Connectomic features underlying diverse synaptic connection strengths and subcellular computation

Tony X. Liu, Pasha A. Davoudian, Kristyn M. Lizbinski, and James M. Jeanne

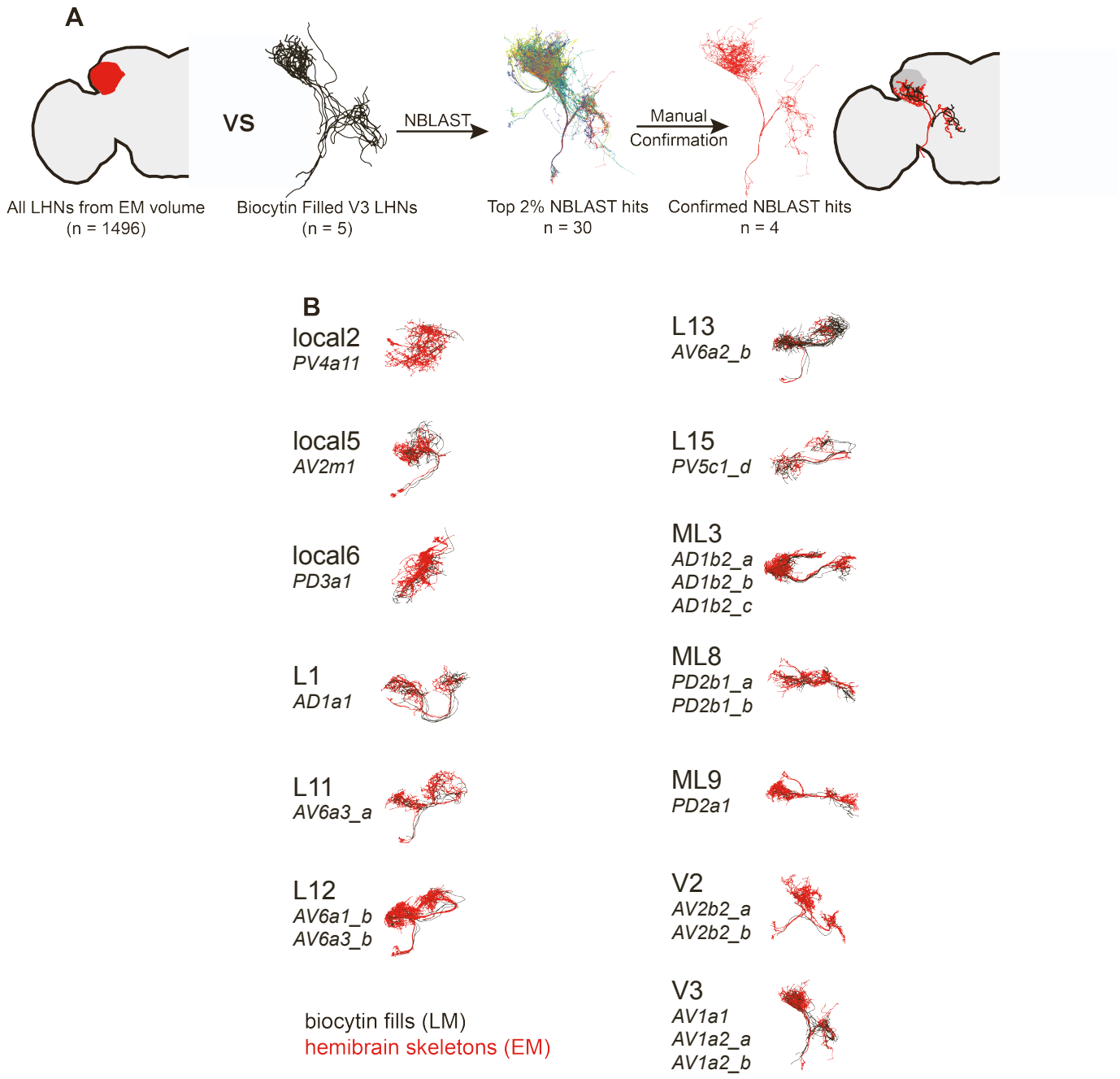

Figure S1: Identifying LHNs between EM and LM data. Related to Figure 1.

(A) Graphical illustration of procedure for finding the same LHN types between EM and LM datasets. We began with the skeletonized morphologies of all 1496 LHNs in the hemibrain connectome. For each LHN type as defined by Jeanne et al.[S1], we collected all skeletonized biocytin fills (the V3 LHN type is illustrated here) and quantitatively compared them to all hemibrain LHNs using the NBLAST algorithm. The highest scoring 30 hits from the hemibrain were selected for expert manual confirmation.

(B) Superimposed representations of biocytin fills for each LHN type (black) and hemibrain skeletons (red). Hemibrain LHN type names are provided in italics. Note that not all bodyIds of each hemibrain type necessarily match to the biocytin fills. See Table S2 for exact matches.

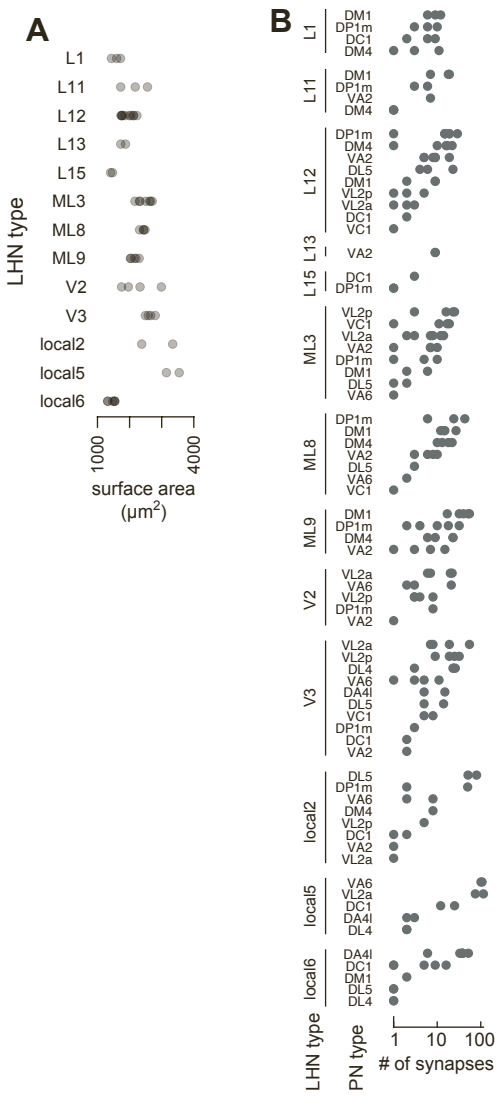

Figure S2: Characteristics of individual LHNs and PN-LHN connections. Related to Figure 1.

(A) LHN types have characteristic surface areas. Each point denotes a single neuron from the hemibrain connectome, grouped by LHN type. Variability between average surface areas across LHN types is greater than within types (ANOVA, $F = 15.2$, $p = 1.8 \times 10^{-11}$).

(B) PN-LHN connections have characteristic synapse counts. Each point denotes a single PN-LHN connection, grouped by connection type. Variability between average synapse counts across types is greater than within types (ANOVA, $F = 15.65$, $p = 2.6 \times 10^{-63}$).

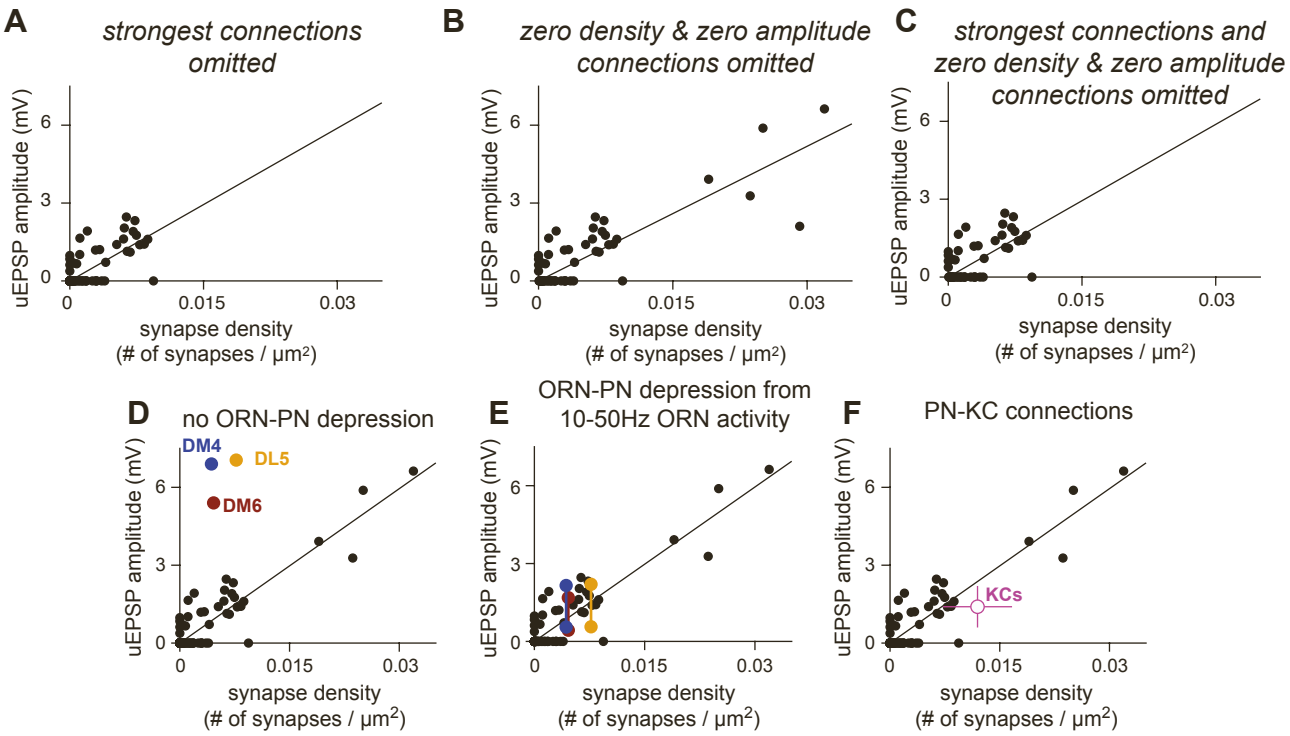

Figure S3: Further analysis of correspondence between anatomy and physiology of connections, and comparison with other types of connection. Related to Figure 3.

(A-C) The correlation between synapse density and uEPSP amplitude persists in the absence of the 5 strongest connections (A; $r^2 = 0.55$, $p = 1.8 \times 10^{-24}$), in the absence of the connections with zero density and zero amplitude (B; $r^2 = 0.72$, $p = 3.8 \times 10^{-18}$), and in the absence of both those sets of connections (C; $r^2 = 0.42$, $p = 4.4 \times 10^{-8}$). Note that a handful of PN-LHN pairs with 0 mV uEPSP amplitude have small (but non-zero) synapse densities, which are evident near the origin of these plots.

To determine whether the relationship we observe between synapse density and uEPSP amplitude for PN-LHN pairs is similar for other classes of neuron, we compared our data to those of two different classes of Drosophila synaptic connections: from olfactory receptor neurons (ORNs) to PNs and from PNs to Kenyon cells (KCs).

(D) uEPSPs for three different ORN-PN connections were analyzed from previously published data[S2] and compared to their corresponding synaptic density measurements, computed using identical methodology as for PN-LHN connections. A fourth ORN-PN connection (VM2) was not analyzed because that glomerulus was partially cut off in the hemibrain EM volume[S3], precluding accurate estimates of surface area for the VM2 PN. The uEPSP amplitudes for each of these ORN-PN connections are much larger than for PN-LHN connections of the same synaptic density. However, ORN-PN synapses experience profound short-term depression and these uEPSPs were measured after long periods of ORN quiescence (via a nerve shock protocol without ORN spontaneous activity)[S2].

(E) To estimate how activity would depress each of these uEPSP amplitudes, as would occur during naturalistic *in vivo* odor-evoked activity, we implemented a simple model of short-term depression previously fit to ORN-PN synaptic connections[S4]. Each ORN was simulated at a rate of 10Hz (top colored points) or 50Hz (bottom colored points), which bracket the average PN stimulation rate of 15Hz in the PN-LHN experiments. At these rates, synaptic depression brings uEPSP amplitudes closer to those predicted from PN-LHN connections.

(F) We compared PN-LHN connections to PN-KC connections. The mean and standard deviation of these uEPSP amplitudes were obtained from published measurements from whole-cell recordings of KCs[S5]. Synapse densities were obtained for all 10,739 connections from the 102 cholinergic uniglomerular PNs onto the 1927 traced KCs reported in the hemibrain connectome. Error bars denote standard deviation. uEPSP amplitudes for PN-KC connections were highly consistent with those for PN-LHN connections, although modestly lower than predicted.

Overall, this comparison indicates that the relationship between synapse density and uEPSP amplitude is broadly similar across cell classes, but also highlights the importance of short-term synaptic plasticity in this relationship.

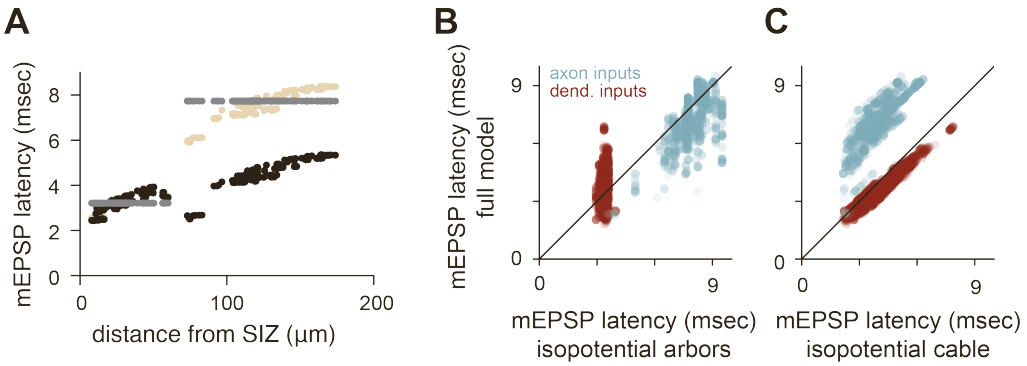

Figure S4: Democratization and division of mEPSP peak latencies. Related to Figure 5.

(A) Latencies to peak mEPSP for all ePN synapses onto the example local5 LHN, as a function of distance from the SIZ (tan). While the most proximal axonal synapses are nearly the same distance from the SIZ as the most distal dendritic synapses (~60 µm), they evoke strikingly different mEPSP latencies. Grey points are the same measurements, but for a model with isopotential arbors. Black points are for a model with an isopotential inter-arbor cable.

(B) Latencies to peak mEPSP simulated with the full model vs. the isopotential arbor model for all synapses across 49 local LHNs.

(C) Latencies to peak mEPSP simulated with the full model vs. the isopotential cable model for all synapses across 49 local LHNs.

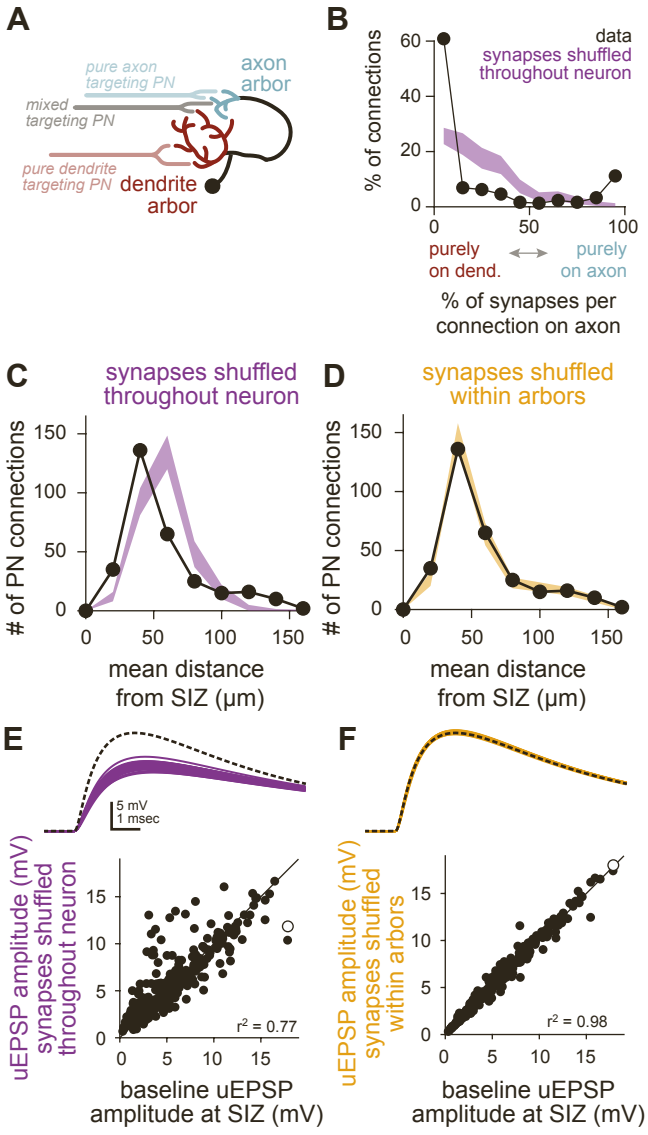

Figure S5. PN connections target synapses to specific arbors but lack sub-arbor organization. Related to Figure 6.

(A) Schematic of PNs targeting axons and dendrites of local LHNs.

(B) Most individual PN connections (with ≥5 synapses) purely target one local LHN arbor or the other. Compared to a null distribution generated by shuffling all PN synapse labels throughout each neuron (purple band denotes the 95% confidence interval), connections are strongly biased towards targeting a single arbor (black points). Most dendrites receive more synapses than axons, so the null distribution skews left.

(C) Arbor-specific targeting of PN connections broadens the distribution of mean distances to the SIZ across connections onto 49 local LHNs. Black points are the true distribution of mean distances for each connection. Purple band denotes the 95% confidence interval for randomly shuffled synapse locations throughout the whole neuron.

(D) As in (C) but compared to a null model of synapse locations shuffled within arbors (orange band: 95% confidence interval).

(E-F) Shuffling synapse locations throughout the neuron (E) perturbs uEPSP amplitudes more than shuffling only within arbors (F). Example uEPSP traces at top (dashed black line denotes trace for real synapse locations; each colored line denotes one shuffle) correspond to open circles in scatter plots below.

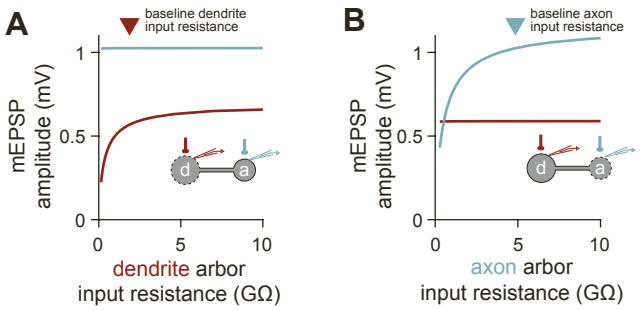

Figure S6: Input resistance of remote arbor does not impact input gain of local arbor. Related to Figure 6.

(A) Changing the dendrite arbor input resistance in the barbell model of an average local LHN does not impact input gain (mEPSP amplitude) in the axon arbor (light blue line), although it does change input gain within the dendrite arbor (red line). In each case, stimulation and measurement occur in the same arbor.

(B) As in (A), but for changing the axon arbor input resistance.

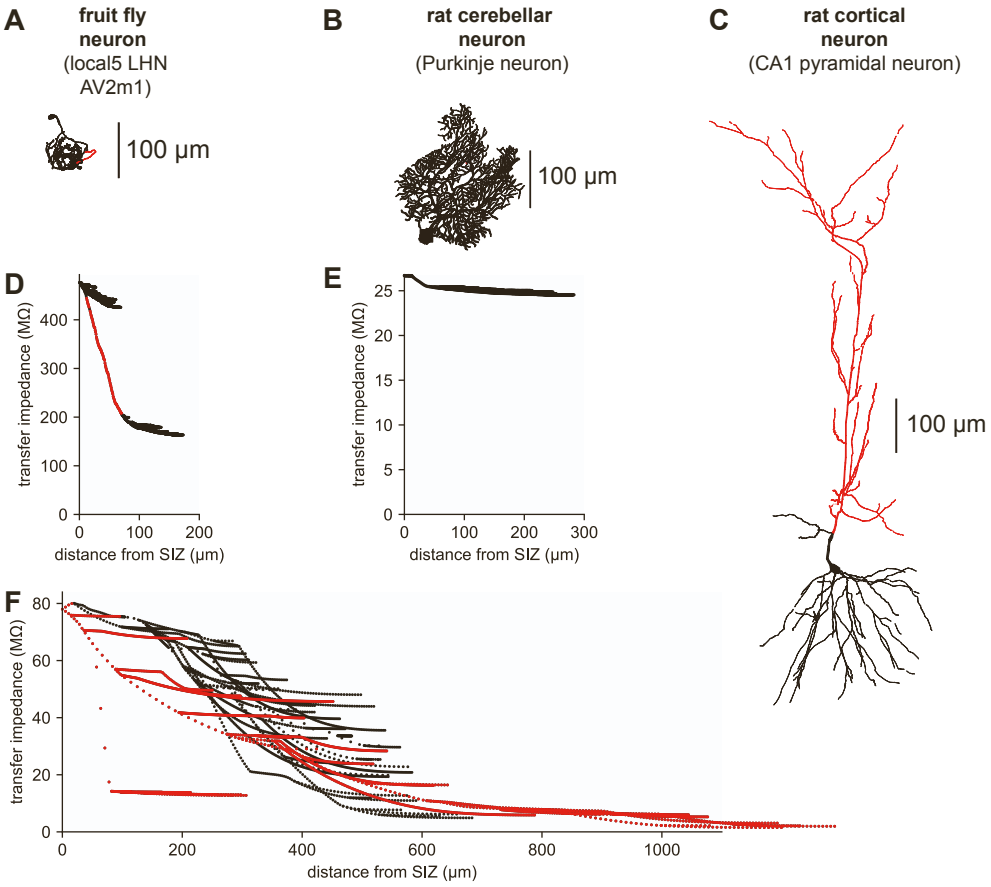

Figure S7: Comparison of transfer impedance profiles across species. Related to Figure 7.
Transfer impedance is a measure of synaptic efficacy, measured as the ratio of voltage at one location to the amount of current injected at another location. We calculated transfer impedance at 20 Hz, to provide a physiologically relevant measure of synaptic efficacy[S6,S7]. All plots are measured from the spike initiation zone, assumed to be at the soma for mammalian neurons.

(A-C) Morphologies of three distinct neuron types.

(D) Transfer impedance profile of a local LHN, local5 (hemibrain type AV2m1). The inter-arbor cable connecting the dendritic (higher transfer impedance) and axonal (lower transfer impedance) arbors is highlighted in red, corresponding to the red segment in (A). Transfer impedance drops rapidly along the inter-arbor cable, while it remains relatively stable within each arbor.

(E) Transfer impedance profile of a rat Purkinje cell dendritic tree[S8]. Transfer impedance is largely constant throughout the entire tree.

(F) Transfer impedance profile of a rat CA1 pyramidal cell[S9]. The apical dendritic subtree is highlighted in red in both the morphological projection (top) and the transfer impedance graph (bottom). Transfer impedance is highly variable across dendritic locations in this cell type.

The individual arbors of the fly neuron and the dendritic arbor of the Purkinje neuron exhibit minimal variability in transfer impedance, creating passive conditions for democratic integration of synaptic inputs. This arises, in part, because their extensive branching creates many relatively short (sealed end) neurites. The high local input impedance of these neurites causes large local depolarizations that largely compensate for the additional cable filtering imposed by their length.

In contrast, transfer impedance drops rapidly along the fly neuron inter-arbor cable and the rat cortical neuron apical dendritic trunk. These long cables (with open ends) exhibit fairly uniform local input resistance along their length, so they mostly cause passive attenuation and are well-approximated by an infinite cable. These minimally branched cables subdivide both fly and rat neurons into compartments with different synaptic efficacies.

Biophysical parameters in the local5 LHN are as in the rest of this study. Parameters for the Purkinje neuron are based on Roth and Hausser[S8]: r_a = 115 Ohm-cm, cm = 0.77 uF/cm2, g_L = 8.2 × 10-6 S/cm^2. Parameters for the CA1 pyramidal neuron are based on Jaffe and Carnevale[S7]: r_a = 200 Ohm-cm, cm = 1.0 uF/cm^2, g_L = 2.2 × 10-5 S/cm^2.

Cell class	Cell type name (Jeanne 2018 nomenclature for LHNs)	hemibrain body ID	hemibrain type	Nblast Score (avg) LHNs only	NBlast Rank (x/1496) LHNs only
PN	DA4l	544021095	DA4l		
PN	DC1	1640594274	DC1		
PN	DL4	1670934213	DL4		
PN	DL5	693483018	DL5		
PN	DM1	542634818	DM1		
PN	DM4	573333835	DM4		
PN	DP1m	635062078	DP1m		
PN	VA2	1977579449	VA2		
PN	VA6	1881751117	VA6		
PN	VC1	606090268	VC1		
PN	VL2a	5813069089	VL2a		
PN	VL2p	1944507292	VL2p		
LHN	L1	454045389	LHAD1a1	0.442261659	1
LHN	L1	483716037	LHAD1a1	0.441719868	2
LHN	L1	575806223	LHAD1a1	0.427799606	3
LHN	L11	329211098	LHAV6a3_a	0.554795813	1
LHN	L11	297921527	LHAV6a3_a	0.52649763	5
LHN	L11	360578457	LHAV6a3_a	0.52471795	7
LHN	L12	5813077898	LHAV6a1_b	0.562373856	1
LHN	L12	579562628	LHAV6a1_b	0.541885823	2
LHN	L12	5813009995	LHAV6a1_b	0.523343252	3
LHN	L12	5813129316	LHAV6a1_b	0.513142148	4
LHN	L12	421957711	LHAV6a3_b	0.504550018	6
LHN	L12	574011220	LHAV6a1_b	0.503113782	7
LHN	L12	603681826	LHAV6a3_b	0.479775282	10
LHN	L12	391609333	LHAV6a3_b	0.470003264	13
LHN	L12	668144344	LHAV6a1_b	0.465230032	15
LHN	L12	392640591	LHAV6a1_b	0.463004577	16
LHN	L13	793702856	LHAV6a2_b	0.45953176	8
LHN	L13	665747387	LHAV6a2_b	0.44875874	10
LHN	L15	5813009429	LHPV5c1_d	0.386832899	21
LHN	L15	422307542	LHPV5c1_d	0.381203242	26
LHN	local2	5813055963	LHPV4a11	0.53015398	1
LHN	local2	666450841	LHPV4a11	0.46242149	2
LHN	local5	5813105722	LHAV2m1	0.561500043	3
LHN	local5	696126258	LHAV2m1	0.521048596	7
LHN	local6	356467849	LHPD3a1	0.38748957	5
LHN	local6	417186656	LHPD3a1	0.369144696	8
LHN	local6	479917037	LHPD3a1	0.358812325	10
LHN	local6	418865948	LHPD3a1	0.35569524	13
LHN	local6	386825553	LHPD3a1	0.334659761	23
LHN	local6	480581806	LHPD3a1	0.319957286	26
LHN	ML3	574040939	LHAD1b2_c	0.486737207	2
LHN	ML3	5813052205	LHAD1b2_c	0.469449144	7
LHN	ML3	483017681	LHAD1b2_b	0.461419557	8
LHN	ML3	573683438	LHAD1b2_b	0.460186168	10
LHN	ML3	543321179	LHAD1b2_c	0.454071541	11
LHN	ML3	5813022459	LHAD1b2_b	0.43781394	18
LHN	ML3	824349873	LHAD1b2_a	0.425080308	29
LHN	ML8	509928512	LHPD2b1_a	0.412211671	2
LHN	ML8	5813089504	LHPD2b1_a	0.361760405	4
LHN	ML8	571666400	LHPD2b1_b	0.335828302	6

LHN	ML8	548872750	LHPD2b1_a	0.304534545	12
LHN	ML9	640963556	LHPD2a1	0.443699058	1
LHN	ML9	573337611	LHPD2a1	0.431549757	2
LHN	ML9	573329304	LHPD2a1	0.42583172	3
LHN	ML9	542634516	LHPD2a1	0.42212864	4
LHN	ML9	571666434	LHPD2a1	0.42147579	5
LHN	V2	1037510115	LHAV2b2_b	0.60558626	1
LHN	V2	5813016204	LHAV2b2_b	0.55008794	4
LHN	V2	852302504	LHAV2b2_a	0.512422657	6
LHN	V2	851961337	LHAV2b2_a	0.43950302	9
LHN	V3	915724147	LHAV1a2_b	0.51923807	1
LHN	V3	883338122	LHAV1a1	0.49128128	2
LHN	V3	789588935	LHAV1a1	0.42919474	5
LHN	V3	917450071	LHAV1a2_a	0.42267591	8

Table S1: Details of matching PN and LHN types. Related to Figure 1.
Listed are each PN and LHN name and corresponding matched hemibrain body ID. For LHNs, both the Jeanne et al.[S1] names and the hemibrain names are provided. For each LHN bodyId the average NBLAST scores (from comparison to each biocytin fill of that type) and NBLAST ranks (out of all 1496 hemibrain LHNs) are also provided.

Connection	mean # of synapses	LHN surface area (μm^2)	mean synapse density (μm^{-2})	mean EPSP amplitude (mV)
'DA4l/L1'	0	1493.5	0	0
'DC1/L1'	5.666667	1493.5	0.0038	NaN
'DL4/L1'	0	1493.5	0	0
'DL5/L1'	0	1493.5	0	0.8422698
'DM1/L1'	9	1493.5	0.006	1.61617573
'DM4/L1'	5	1493.5	0.0033	1.20671994
'DP1m/L1'	6.333333	1493.5	0.0042	NaN
'VA2/L1'	0	1493.5	0	NaN
'VA6/L1'	0	1493.5	0	0
'VC1/L1'	0	1493.5	0	0
'VL2a/L1'	0	1493.5	0	0
'VL2p/L1'	0	1493.5	0	0
'DA4l/L11'	0	2063.2	0	0
'DC1/L11'	0	2063.2	0	0
'DL4/L11'	0	2063.2	0	0
'DL5/L11'	0	2063.2	0	0
'DM1/L11'	14.66667	2063.2	0.0071	1.90507386
'DM4/L11'	1	2063.2	0.0005	0
'DP1m/L11'	3	2063.2	0.0015	0
'VA2/L11'	2.333333	2063.2	0.0011	1.64688543
'VA6/L11'	0	2063.2	0	0
'VC1/L11'	0	2063.2	0	0
'VL2a/L11'	0	2063.2	0	0
'VL2p/L11'	0	2063.2	0	0
'DA4l/L12'	0	1848.6	0	0
'DC1/L12'	0.2	1848.6	0.0001	0
'DL4/L12'	0	1848.6	0	0
'DL5/L12'	3.3	1848.6	0.0018	0
'DM1/L12'	2	1848.6	0.0011	0
'DM4/L12'	6.6	1848.6	0.0036	0
'DP1m/L12'	11.3	1848.6	0.0061	2.03873945
'VA2/L12'	5.5	1848.6	0.003	0
'VA6/L12'	0	1848.6	0	0
'VC1/L12'	0.1	1848.6	0.0001	0
'VL2a/L12'	0.6	1848.6	0.0003	0
'VL2p/L12'	0.8	1848.6	0.0004	0.68786344
'DA4l/L15'	0	1349.1	0	0
'DC1/L15'	1.5	1349.1	0.0011	1.01693282
'DL4/L15'	0	1349.1	0	0
'DL5/L15'	0	1349.1	0	0
'DM1/L15'	0	1349.1	0	0
'DM4/L15'	0	1349.1	0	0
'DP1m/L15'	1	1349.1	0.0007	0
'VA2/L15'	0	1349.1	0	0.9789831
'VA6/L15'	0	1349.1	0	0
'VC1/L15'	0	1349.1	0	NaN
'VL2a/L15'	0	1349.1	0	NaN
'VL2p/L15'	0	1349.1	0	0
'DA4l/local2'	0	2770.7	0	0
'DC1/local2'	1.5	2770.7	0.0005	0
'DL4/local2'	0	2770.7	0	0
'DL5/local2'	65.5	2770.7	0.0236	3.27651952
'DM1/local2'	0	2770.7	0	0
'DM4/local2'	4	2770.7	0.0014	0
'DP1m/local2'	26	2770.7	0.0094	0
'VA2/local2'	0.5	2770.7	0.0002	0

'VA6/local2'	5	2770.7	0.0018	0
'VC1/local2'	0	2770.7	0	0
'VL2a/local2'	0.5	2770.7	0.0002	NaN
'VL2p/local2'	2.5	2770.7	0.0009	NaN
'DA4l/local5'	2.5	3256.7	0.0008	0.65942807
'DC1/local5'	18.5	3256.7	0.0057	NaN
'DL4/local5'	2	3256.7	0.0006	0
'DL5/local5'	0	3256.7	0	NaN
'DM1/local5'	0	3256.7	0	NaN
'DM4/local5'	0	3256.7	0	0
'DP1m/local5'	0	3256.7	0	NaN
'VA2/local5'	0	3256.7	0	0
'VA6/local5'	104	3256.7	0.0319	6.62604114
'VC1/local5'	0	3256.7	0	0
'VL2a/local5'	95	3256.7	0.0292	2.104459
'VL2p/local5'	0	3256.7	0	0.61719868
'DA4l/local6'	34.16667	1363	0.0251	5.88633018
'DC1/local6'	5.333333	1363	0.0039	0
'DL4/local6'	0.333333	1363	0.0002	0
'DL5/local6'	0.333333	1363	0.0002	0
'DM1/local6'	0.333333	1363	0.0002	0
'DM4/local6'	0	1363	0	0
'DP1m/local6'	0	1363	0	0
'VA2/local6'	0	1363	0	0
'VA6/local6'	0	1363	0	0
'VC1/local6'	0	1363	0	0
'VL2a/local6'	0	1363	0	0
'VL2p/local6'	0	1363	0	0
'DA4l/ML3'	0	2379.8	0	0
'DC1/ML3'	0	2379.8	0	0
'DL4/ML3'	0	2379.8	0	0
'DL5/ML3'	0.428571	2379.8	0.0002	NaN
'DM1/ML3'	1.142857	2379.8	0.0005	0
'DM4/ML3'	0	2379.8	0	0
'DP1m/ML3'	2.285714	2379.8	0.001	0
'VA2/ML3'	3.571429	2379.8	0.0015	NaN
'VA6/ML3'	0.142857	2379.8	0.0001	NaN
'VC1/ML3'	6.857143	2379.8	0.0029	1.18859636
'VL2a/ML3'	6.571429	2379.8	0.0028	NaN
'VL2p/ML3'	9.571429	2379.8	0.004	0.71611048
'DA4l/ML8'	0	2327	0	0
'DC1/ML8'	0	2327	0	0
'DL4/ML8'	0	2327	0	0
'DL5/ML8'	0.75	2327	0.0003	NaN
'DM1/ML8'	17	2327	0.0073	2.32240857
'DM4/ML8'	15.75	2327	0.0068	1.10980746
'DP1m/ML8'	18.25	2327	0.0078	1.39218545
'VA2/ML8'	6.75	2327	0.0029	0
'VA6/ML8'	0.5	2327	0.0002	0
'VC1/ML8'	0.25	2327	0.0001	0
'VL2a/ML8'	0	2327	0	0
'VL2p/ML8'	0	2327	0	0
'DA4l/ML9'	0	2052.8	0	0
'DC1/ML9'	0	2052.8	0	0
'DL4/ML9'	0	2052.8	0	0
'DL5/ML9'	0	2052.8	0	0
'DM1/ML9'	39	2052.8	0.019	3.91653936
'DM4/ML9'	12.2	2052.8	0.0059	NaN
'DP1m/ML9'	13.2	2052.8	0.0064	1.14060981

'VA2/ML9'	5.2	2052.8	0.0025	0
'VA6/ML9'	0	2052.8	0	0
'VC1/ML9'	0	2052.8	0	0
'VL2a/ML9'	0	2052.8	0	0
'VL2p/ML9'	0	2052.8	0	NaN
'DA4l/V2'	0	2168.1	0	0
'DC1/V2'	0	2168.1	0	0
'DL4/V2'	0	2168.1	0	0
'DL5/V2'	0	2168.1	0	0
'DM1/V2'	0	2168.1	0	0
'DM4/V2'	0	2168.1	0	0
'DP1m/V2'	2	2168.1	0.0009	NaN
'VA2/V2'	0.25	2168.1	0.0001	0
'VA6/V2'	6.5	2168.1	0.003	0
'VC1/V2'	0	2168.1	0	0
'VL2a/V2'	13.75	2168.1	0.0063	2.46240283
'VL2p/V2'	4.5	2168.1	0.0021	NaN
'DA4l/V3'	5	2544.5	0.002	NaN
'DC1/V3'	0.5	2544.5	0.0002	0
'DL4/V3'	19	2544.5	0.0075	1.75984939
'DL5/V3'	4.75	2544.5	0.0019	0
'DM1/V3'	0	2544.5	0	0
'DM4/V3'	0	2544.5	0	0
'DP1m/V3'	0.75	2544.5	0.0003	0
'VA2/V3'	0.5	2544.5	0.0002	0
'VA6/V3'	5	2544.5	0.002	1.92217112
'VC1/V3'	3.25	2544.5	0.0013	0
'VL2a/V3'	22.25	2544.5	0.0087	1.60422109
'VL2p/V3'	21.25	2544.5	0.0084	1.41590037
'DA4l/L13'	0	1710.7	0	0
'DC1/L13'	0	1710.7	0	0
'DL4/L13'	0	1710.7	0	0
'DL5/L13'	0	1710.7	0	0.37863795
'DM1/L13'	0	1710.7	0	0
'DM4/L13'	0	1710.7	0	0
'DP1m/L13'	0	1710.7	0	0
'VA2/L13'	9	1710.7	0.0053	1.4024964
'VA6/L13'	0	1710.7	0	0
'VC1/L13'	0	1710.7	0	0
'VL2a/L13'	0	1710.7	0	0
'VL2p/L13'	0	1710.7	0	0

Table S3: Synapse densities and uEPSP amplitudes for each PN-LHN pair. Related to Figure 3.
Connections with uEPSP amplitudes listed as “NaN” are those which were not reliable or measurable in the data and were therefore excluded from all analysis (STAR Methods).

Supplemental References

S1. Jeanne, J.M., Fisek, M., and Wilson, R.I. (2018). The organization of projections from olfactory glomeruli onto higher-order neurons. Neuron *98*, 1198-1213.

S2. Kazama, H., and Wilson, R.I. (2008). Homeostatic matching and nonlinear amplification at genetically-identified central synapses. Neuron *58*, 401-413.

S3. Schlegel, P., Bates, A.S., Sturner, T., Jagannathan, S.R., Drummond, N., Hsu, J., Serratosa Capdevila, L., Javier, A., Marin, E.C., Barth-Maron, A., et al. (2021). Information flow, cell types and stereotypy in a full olfactory connectome. Elife *10*, e66018.

S4. Nagel, K.I., Hong, E.J., and Wilson, R.I. (2015). Synaptic and circuit mechanisms promoting broadband transmission of olfactory stimulus dynamics. Nat. Neurosci. *18*, 56-65.

S5. Turner, G.C., Bazhenov, M., and Laurent, G. (2008). Olfactory representations by Drosophila mushroom body neurons. J. Neurophysiol. *99*, 734-746.

S6. Chitwood, R.A., Hubbard, A., and Jaffe, D.B. (1999). Passive electrotonic properties of rat hippocampal CA3 interneurones. J. Physiol. *515 (Pt 3)*, 743-756.

S7. Jaffe, D.B., and Carnevale, N.T. (1999). Passive normalization of synaptic integration influenced by dendritic architecture. J. Neurophysiol. *82*, 3268-3285.

S8. Roth, A., and Hausser, M. (2001). Compartmental models of rat cerebellar Purkinje cells based on simultaneous somatic and dendritic patch-clamp recordings. J. Physiol. *535*, 445-472.

S9. Pyapali, G.K., and Turner, D.A. (1996). Increased dendritic extent in hippocampal CA1 neurons from aged F344 rats. Neurobiol Aging *17*, 601-611.